

Magnetic characteristics of epitaxial NiO films studied by Raman spectroscopy

J. Feldl,^{1, a)} M. Budde,¹ C. Tschammer,¹ O. Bierwagen,¹ and M. Ramsteiner^{1, b)}

Paul-Drude-Institut für Festkörperelektronik, Leibniz-Institut im Forschungsverbund Berlin e. V., Hausvogteiplatz 5–7, 10117 Berlin, Germany

Raman spectroscopy is utilized to study the magnetic characteristics of heteroepitaxial NiO thin films grown by plasma-assisted molecular beam epitaxy on MgO(100) substrates. For the determination of the Néel temperature, we demonstrate a reliable approach by analyzing the temperature dependence of the Raman peak originating from second-order scattering by magnons. The antiferromagnetic coupling strength is found to be strongly influenced by the growth conditions. The low-temperature magnon frequency and the Néel temperature are demonstrated to depend on the biaxial lattice strain and the degree of structural disorder which is dominated by point defects.

I. INTRODUCTION

NiO is one of the rare transparent oxides (bandgap around 3.7 eV) which can be utilized as a *p*-type semiconductor.^{1–3} Furthermore, as one of the most common antiferromagnetic oxides (with an antiferromagnetic to paramagnetic phase-transition at a Néel temperature of 523 K) NiO is of interest for both fundamental studies and spintronic applications.^{4,5} NiO has a rock salt structure with ferromagnetic alignment of the magnetic moments in each {111} plane and antiferromagnetic coupling between neighboring {111} planes via a Ni-O super exchange interaction.⁶ Thereby, the next-nearest-neighbor (180°) Ni⁺²-O⁻²-Ni⁺² antiferromagnetic exchange *J* is much larger than the nearest-neighbor (90°) ferromagnetic exchange making the latter one negligible.⁷ However, in thin magnetic films synthesized by various methods, the ferromagnetic or antiferromagnetic coupling is expected to be modified and deteriorated by disorder and strain as reported previously for ferromagnetic manganites.⁸ Regarding lattice strain, a well-defined influence on the magnetic characteristics is expected based on results obtained by measurements under hydrostatic pressure.⁷ For the experimental investigation of structural and magnetic properties, Raman spectroscopy of phonons and magnons in NiO^{7,9–23} and other antiferromagnetic materials^{9,24–27} has been proven to be a powerful method. In addition to the Raman spectroscopic work, theoretical studies^{28–32} on phonons and magnons in NiO as well as investigations based on other experimental techniques^{6,33–35} can be found in the literature.

In this work, Raman spectroscopy is demonstrated as a tool to investigate both the structural and magnetic characteristics of NiO thin films. As a result, we reveal that the low-temperature magnon frequency and the Néel temperature depend not only on the biaxial misfit strain but also on structural disorder in the epitaxial NiO films.

II. EXPERIMENTAL DETAILS

The investigated NiO samples were grown on MgO(100) substrates by plasma-assisted molecular beam epitaxy. Be-

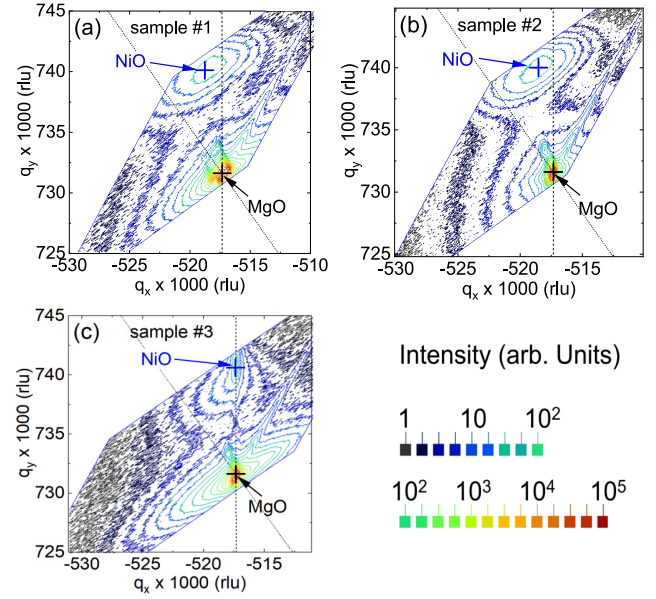


FIG. 1. X-ray diffraction reciprocal space maps around the 422 reflection of (a) sample #1 grown at 700 °C, (b) sample #2 grown at 200 °C and (c) sample #3 grown at 20 °C. The maps are drawn by equiintensity lines using a color coded, logarithmic scale as specified. The numerically extracted peak positions of the MgO substrate and the thin NiO films are marked by black and blue crosses, respectively, and labeled accordingly. The unit rlu is defined as $\lambda/2d$ with x-ray wavelength λ and spacing of the lattice planes d . q_x and q_y correspond to the in-plane (022) and out-of plane (400) components of the investigated reflection. A NiO peak on the vertical dashed or oblique dotted line corresponds to pseudomorphically strained or fully relaxed layers, respectively.

cause of the common rock-salt crystal structure and the similar lattice constants of MgO (0.4212 nm) and NiO (0.4176 nm), MgO is a widely used, suitable substrate for the growth of high quality NiO films.³ Covering a large range of substrate temperatures, the investigated films were grown at 700 °C (sample #1), 200 °C (sample #2) and 20 °C (sample #3). These samples correspond to S2-700, S2-200 and S2-20 of Ref. 23. Films grown at higher substrate temperatures exhibit Ni_xMg_{1-x}O alloying. From the chosen growth conditions and the previous characterization of the NiO films, the existence of secondary phases and a significant impact of surface roughness can be excluded for all samples (see

^{a)}Electronic mail: feldl@pdi-berlin.de

^{b)}Electronic mail: ramsteiner@pdi-berlin.de

Ref. 23). The investigated single crystalline thin NiO films have thicknesses of about 60 nm, a close-to-stoichiometric composition and exhibit optical transparency in the visible spectral range. For reference purposes, an about 0.7 mm thick green NiO foil has been utilized as a bulk-like sample. This sample has been characterized previously by x-ray diffraction, spectroscopic ellipsometry and Raman spectroscopy (see Ref. 23). The results reveal that our reference sample can be regarded as unstrained bulk NiO with state-of-the-art quality. The occurrence of a weak Raman-forbidden peak at 580 cm^{-1} (see Fig. 2) is commonly observed for single crystalline NiO.^{15,17,21}

The in-plane and out-of-plane lattice parameters of the thin NiO films were determined by x-ray diffraction reciprocal space mapping (RSM). The corresponding RSMs were taken around the 422 reflection in asymmetric geometry by a four-circle lab-diffractometer (PANalytical X'Pert Pro MRD) using a line detector (Pixcel, 256 channels covering a 2Θ -range of 2.51°) and $\text{Cu K}\alpha$ radiation.

The Raman spectroscopic measurements were performed in the backscattering configuration with optical excitation at wavelengths of 405 nm (solid-state laser) and 325 nm (He-Cd laser). The incident laser light was focused by a microscope objective onto the sample surface (spot diameter of approximately $2\ \mu\text{m}$). The backscattered light was collected by the same objective (confocal configuration), spectrally dispersed by an 80-cm spectrograph (LabRam HR Evolution, Horiba/Jobin Yvon) and detected with a liquid-nitrogen-cooled charge-coupled device (CCD). For Rayleigh light suppression, a bandpass filter with ultra-narrow spectral bandwidth was used. For the temperature dependent Raman scattering measurements, a continuous-flow cryostat (CryoVac) and a heating stage (Linkam) were used in the temperature ranges of 10–300 K and 300–550 K, respectively.

III. RESULTS AND DISCUSSION

A. Lattice strain

Figure 1 shows the RSMs of the thin NiO films. The in-plane (a) and out-of-plane (c) lattice parameters of the NiO films, extracted from these maps using the relation $q = \lambda/2d$ with wavelength λ and spacing of the crystal planes ($d_{400} = c/4$, $d_{022} = a/\sqrt{8}$), are shown in Table I. Interestingly, growth at 20°C resulted in a pseudomorphically strained NiO layer, indicated by the coinciding in-plane lattice parameter (same q_x) of NiO film and MgO substrate in Fig. 1(c). Higher growth temperatures of 200°C and 700°C , in contrast, resulted in the growth of thin NiO films that are partially relaxed (towards the smaller lattice parameter of NiO than that of MgO), indicated by larger magnitude q_x of the layer compared to that of the substrate in Fig. 1(b,a).

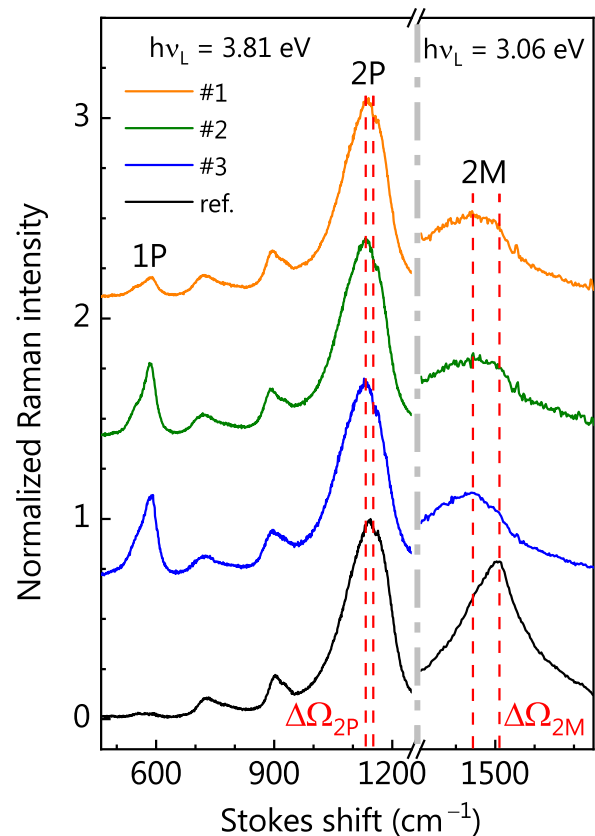


FIG. 2. Room temperature Raman spectra of the thin NiO films and a reference bulk NiO sample excited at 3.81 eV (lower frequency range) and 3.06 eV (frequency range above 1220 cm^{-1}).

TABLE I. Substrate growth temperature T_S , in- and out-of-plane lattice parameter a and c as well as the quality index 1–Q for the bulk reference and samples #1 to #3.

| Sample | T_S ($^\circ\text{C}$) | a (\AA) | c (\AA) | 1 – Q |
|--------|----------------------------|----------------------|----------------------|-------|
| ref. | N/A | 4.178 | 4.178 | 0.97 |
| #1 | 700 | 4.200 | 4.163 | 0.88 |
| #2 | 200 | 4.201 | 4.164 | 0.81 |
| #3 | 20 | 4.211 | 4.160 | 0.77 |

B. Structural disorder

Figure 2 displays room temperature Raman spectra of the thin NiO films and the reference bulk NiO sample. Optical excitation at 3.81 eV (325 nm) close to the NiO bandgap was used for the lower frequency range (up to 1220 cm^{-1}). This condition enables a high sensitivity for optical-phonon scattering due to resonance-enhanced Raman scattering. The corresponding spectrum of bulk NiO exhibits only peaks due to second-order phonon scattering at 730 , 900 , and 1130 cm^{-1} (2P) in agreement with the forbidden first-order Raman scattering by optical phonons in the rock-salt structure.^{9,21} In contrast, the thin NiO films reveal

also first-order Raman scattering at 580 cm^{-1} (1P).^{15,21} As a further deviation from the spectrum of bulk NiO, the 2P peak of the thin NiO films is shifted to lower frequencies. This redshift $\Delta\Omega_{2P}$ is attributed to biaxial strain in the thin NiO films.

Since the occurrence of the Raman peak 1P is enabled by a deviation from the perfect lattice order, we have defined a quality index Q as an inverse figure of merit for the crystal quality:²³

$$Q = \frac{I_{1P}}{I_{2P}}. \quad (1)$$

Here, I_{1P} and I_{2P} denote the intensity of the 1P and 2P Raman peaks, respectively. Note that $Q = 0$ corresponds to a perfect NiO crystal with rock-salt structure and $1 - Q$ reflects the degree of structural order in NiO. As shown in Fig. 3, the magnitude of $1 - Q$ decreases monotonically with the tensile in-plane strain determined from the data shown in Table I assuming a lattice parameter of 4.176 \AA for bulk NiO. Since the pseudomorphically strained film (sample #3) exhibits the lowest crystal quality $1 - Q$, our result indicates that the lattice disorder in the thin NiO films is dominated by point defects rather than by misfit dislocations induced by partial relaxation of the misfit strain (in samples #1 and #2). In fact, oxygen rich growth conditions lead to the creation of acceptor-like Ni vacancies in NiO films.³ Furthermore, low growth temperatures favor the formation of additional point defects or defect complexes as demonstrated in Ref. 36 for NiO films synthesized by pulsed laser deposition. Consequently, it is reasonable to attribute the decreasing magnitude of $1 - Q$ at low growth temperatures (see Table I) to an increasing density of point defects. The opposite strain-dependence of $1 - Q$ can be observed for thin NiO films grown on c-plane GaN substrates,³⁷ as shown in the inset of Fig. 3. This finding confirms that the quantity $1 - Q$ indeed mainly reflects the crystal quality independent of the lattice distortion induced by the biaxial misfit strain.^{23,37}

C. Magnetic characteristics

For the investigation of temperature-dependent second-order Raman scattering by magnons, non-resonant optical excitation at 3.06 eV is used in order to obtain a comparable signal strength for second-order phonon and magnon scattering. The corresponding room temperature Raman spectra shown in Fig. 2 clearly reveal the presence of the second-order magnon peak (2M) at about 1450 cm^{-1} for both, the bulk NiO sample and the thin NiO films.^{7,9} However, the intensity of the 2M peak of the present thin NiO films is reduced (as verified by polarization dependent Raman¹⁷ measurements) and its position is shifted by $\Delta\Omega_{2M}$ to lower frequencies. Both findings are explained by a reduction in the antiferromagnetic coupling via Ni-O super exchange interaction.¹⁵ Note that for the above mentioned thin NiO films grown on GaN or nanosized NiO prepared by a plasma synthesis, no 2M peaks could be resolved in the Raman spectra at room temperature and, therefore, no signature of antiferromagnetism.^{15,37}

An important characteristic of antiferromagnets is the Néel temperature (T_N). In order to determine T_N for the investigated thin NiO films, we take advantage of the common relationship

$$\frac{\Omega_{2M}^0 - \Omega_{2M}(T)}{\Omega_{2M}^0} = \theta \exp\left(\beta \frac{T}{T_N}\right) \quad (2)$$

between the relative shift of the temperature dependent 2M peak $[\Omega_{2M}^0 - \Omega_{2M}(T)]/\Omega_{2M}^0$ and the reduced temperature T/T_N with constant values of θ and β . Ω_{2M}^0 is the respective low-temperature saturation value of the 2M peak frequency. This relationship has been demonstrated previously for different antiferromagnets (NiO and KNiF₃).⁹ In Fig. 4 we show $[\Omega_{2M}^0 - \Omega_{2M}(T)]/\Omega_{2M}^0$ as a function of T/T_N for bulk NiO and the three thin NiO films. In the range $0.5 \leq T/T_N \leq 1.0$, all data points indeed follow the function given in Eq. 2. Within our approach, we first determine the parameters θ and β by fitting the data of the reference bulk sample, keeping the well-known value of $T_N = 523 \text{ K}$ fixed (see Eq. 2). The obtained values θ and β are then used for the fits of the data from individual thin NiO films with T_N as the only free parameter. The excellent agreement between the data and the function given by Eq. 2 demonstrates the consistency and reliability of our approach for the determination of the Néel temperature, an achievement which would otherwise be difficult to attain. The obtained values of T_N for samples #1, #2 and #3 are 481 K , 471 K and 467 K , respectively.

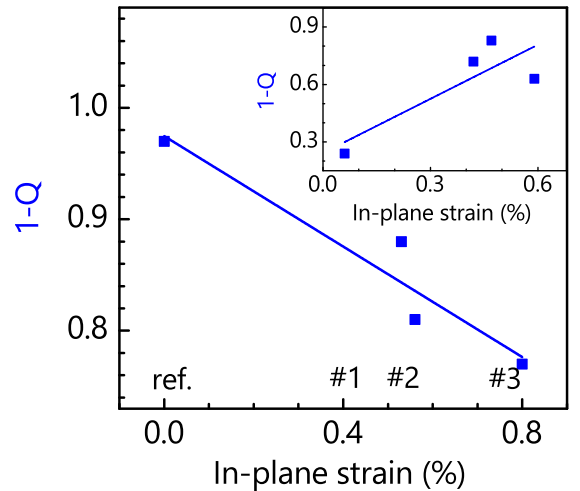


FIG. 3. Degree of structural order $1 - Q$ for bulk NiO (ref.) and all three thin NiO films (samples #1, #2, #3) as a function of the in-plane strain. The inset shows $1 - Q$ for thin NiO films grown on GaN substrates. The straight lines are guides for the eye.

Fig. 5(a) displays the shift of the low-temperature 2M peak frequency ($\Delta\Omega_{2M}^0 = \Omega_{2M}^{0,\text{film}} - \Omega_{2M}^{0,\text{bulk}}$) as well as the shift of the Néel temperature (ΔT_N) as a function of the separation d_{111} between $\{111\}$ lattice planes which is the crucial distance regarding the strength of the antiferromagnetic super exchange interaction. Please note: Since the thin NiO films are grown in (100) direction, the $\{111\}$ plane is not parallel

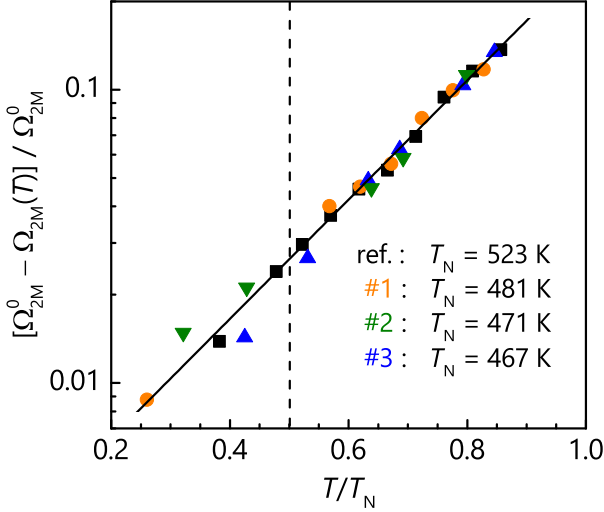


FIG. 4. Relative frequency shift of the 2M peak $[\Omega_{2M}^0 - \Omega_{2M}(T)]/\Omega_{2M}^0$ for bulk NiO (ref.) and the thin NiO films (samples #1, #2, #3) as a function of the reduced temperature T/T_N . The values of T_N for the three thin NiO films have been determined as described in the text. The solid line represents the function $\theta \exp(\beta T/T_N)$ with $\theta = 2.54 \times 10^{-3}$ and $\beta = 4.68$. The fit was performed in the range $0.5 \leq T/T_N \leq 1.0$ as indicated by the dashed line.

to the sample surface. From the known in-plane lattice parameter a and out-of-plane lattice parameters c , the spacing of the $\{111\}$ planes for a tetragonally distorted unit cell can be calculated by

$$d_{hkl} = \left\{ \frac{1}{a^2} (h^2 + k^2) + \frac{1}{c^2} l^2 \right\}^{-\frac{1}{2}}, \quad (3)$$

with $h = k = l = 1$.

As can be clearly seen in Fig. 5(a), both quantities describing the magnetic characteristics ($\Delta\Omega_{2M}^0$ and ΔT_N) exhibit a nearly linear dependence on d_{111} . Since Ω_{2M}^0 and T_N are both proportional to the antiferromagnetic exchange constant J , the observed monotonic relationships with the distance between the antiferromagnetically coupled $\{111\}$ lattice planes constitutes the expected behavior:⁷

$$\frac{\hbar\Omega_{2M}^0}{k_B T_N} = \frac{\alpha}{\gamma} \quad \text{with} \quad (4)$$

$$\hbar\Omega_{2M}^0 = \alpha J \quad \text{and} \quad k_B T_N = \gamma J, \quad (5)$$

where α and γ are proportionality constants.

For thin epitaxial films the crucial question is whether or not the deviation from bulk NiO is caused by the lattice strain alone. As a matter of fact, the comparison to results obtained for bulk NiO under hydrostatic pressure⁷ reveals that the magnitude of the observed shifts shown in Fig. 5(a) cannot be explained only by the biaxial strain in the films [see shift of the Néel temperature expected according to Ref. 7

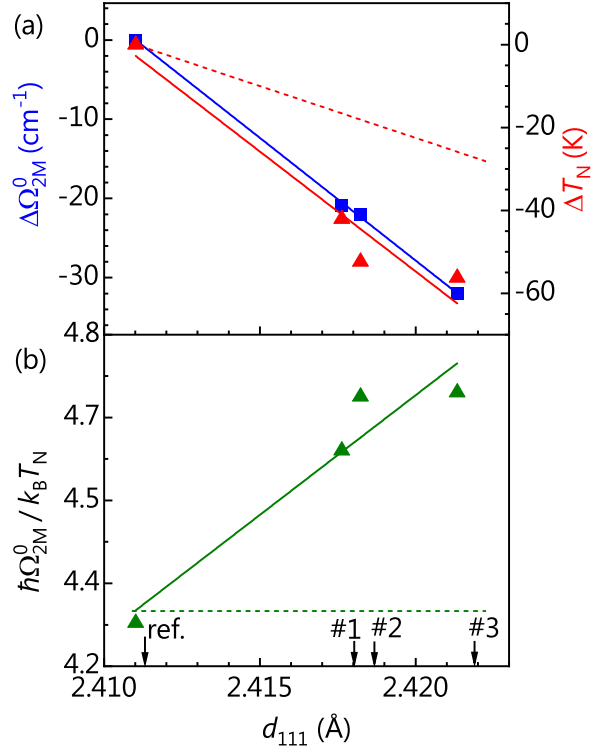


FIG. 5. (a) Shift of the low-temperature 2M peak frequency $\Delta\Omega_{2M}^0$ as well as shift of the Néel temperature ΔT_N for bulk NiO (ref.) and all three thin NiO films (samples #1, #2, #3) as a function of the $\{111\}$ plane spacing. The shift of the Néel temperature according to Ref. 7 is shown for comparison (dashed line). (b) Ratio $\hbar\Omega_{2M}^0 / k_B T_N$ for bulk NiO (ref.) and all three thin NiO films (samples #1, #2, #3) as a function of the $\{111\}$ plane spacing. The constant ratio according to Ref. 7 is shown for comparison (dashed line).

shown in Fig. 5(a) for comparison]. Furthermore, as shown in Fig. 5(b), the ratio $\hbar\Omega_{2M}^0 / k_B T_N$ does not maintain the expected constant value α/γ (cf. Eq. 4) for a super exchange interaction that depends only on the lattice strain⁷, as indicated by the dotted line. This finding indicates that Ω_{2M}^0 and T_N , i.e., the proportionality constants α and γ (cf. Eq. 5), depend in different manners on the growth conditions.

In order to explain the observed variation of the magnetic characteristics, we recall that the magnitude of $1 - Q$ of the thin NiO films decreases with increasing in-plane strain (cf. Fig. 3) and, therefore, also the distance between $\{111\}$ planes. Consequently, we conclude that also the increasing lattice disorder contributes to the decrease in the antiferromagnetic exchange constant J . As already mentioned above, the disorder in the thin NiO films on MgO substrates is most likely dominated by point defects which, in general, are expected to have a strong impact on the antiferromagnetic exchange between Ni^{+2} ions mediated by oxygen orbitals.⁶ Consequently, the antiferromagnetic coupling becomes increasingly disturbed by a growing concentration of point defects. Our results indicate that the impact on the low-temperature magnon frequency is different from that on the

Néel temperature (see Eq. 4 and Fig. 5). Further work is necessary to explain this behavior.

IV. SUMMARY AND CONCLUSIONS

In summary, Raman spectroscopy is demonstrated as a method to evaluate the magnetic characteristics of thin NiO films including a reliable approach for the determination of the Néel temperature. The influence of the growth conditions on the low-temperature magnon frequency and the Néel temperature is explained by the variation of the spacing between {111} lattice planes due to biaxial lattice strain and a significant contribution of lattice disorder introduced by point defects, induced by low growth temperatures. Our results show that besides strain adjustment, e.g. by the proper choice of substrates, also the growth temperature can be used to engineer T_N .

ACKNOWLEDGMENTS

We thank R. Goldhahn and M. Feneberg for providing the bulk NiO reference sample as well as Alberto Hernández-Mínguez for critically reading the manuscript. This work was performed in the framework of GraFOx, a Leibniz-ScienceCampus partially funded by the Leibniz association. J. F. and M. B. gratefully acknowledge the financial support by the Leibniz association.

- ¹H. Ohta, M. Kamiya, T. Kamiya, M. Hirano, and H. Hosono, *Thin Sol. Films* **445**, 317 (2003).
- ²K. V. Rao and A. Smakula, *J. Appl. Phys.* **36**, 2031 (1965).
- ³J. Y. Zhang, W. W. Li, R. L. Z. Hoye, J. L. MacManus-Driscoll, M. Budde, O. Bierwagen, L. Wang, Y. Du, M. J. Wahila, L. F. J. Piper, T.-L. Lee, H. J. Edwards, V. R. Dhanak, and K. H. L. Zhang, *J. Mater. Chem. C* **6**, 2275 (2018).
- ⁴M. Pinarbasi, S. Metin, H. Gill, M. Parker, B. Gurney, M. Carey, and C. Tsang, *J. Appl. Phys.* **87**, 5714 (2000).
- ⁵T. Moriyama, K. Oda, T. Ohkochi, M. Kimata, and T. Ono, *Sci. Rep.* **8**, 14167 (2018), [arXiv:1708.07682](https://arxiv.org/abs/1708.07682).
- ⁶M. T. Hutchings and E. J. Samuelsen, *Phys. Rev. B* **6**, 3447 (1972).
- ⁷M. J. Massey, N. H. Chen, J. W. Allen, and R. Merlin, *Phys. Rev. B* **42**, 8776 (1990).
- ⁸K. Dörr, *J. Phys. D: Appl. Phys.* **39**, R125 (2006).
- ⁹R. E. Dietz, G. I. Parisot, and A. E. Meixner, *Phys. Rev. B* **4**, 2302 (1971).
- ¹⁰R. E. Dietz, W. F. Brinkman, A. E. Meixner, and H. J. Guggenheim, *Phys. Rev. Lett.* **27**, 814 (1971).
- ¹¹D. J. Lockwood, M. G. Cottam, and J. H. Baskey, *J. Magn. Magn. Mater.* **104-107**, 1053 (1992).
- ¹²M. Pressl, M. Mayer, P. Knoll, S. Lo, U. Hohenester, and E. Holzinger-Schweiger, *J. Raman Spectrosc.* **27**, 343 (1996).
- ¹³M. Grimsditch, L. E. McNeil, and D. J. Lockwood, *Phys. Rev. B* **58**, 14462 (1998).
- ¹⁴Y. Mita, Y. Ishida, M. Kobayashi, and S. Endo, *J. Phys. Condens. Matter* **14**, 11173 (2002).
- ¹⁵N. Mironova-Ulmane, A. Kuzmin, I. Steins, J. Grabis, I. Sildos, and M. Pärs, *J. Phys. Conf. Ser.* **93**, 012039 (2007).
- ¹⁶A. Gandhi, C.-Y. Huang, C. Yang, T. Chan, C.-L. Cheng, Y.-R. Ma, and S. Wu, *Nanoscale Res. Lett.* **6**, 485 (2011).
- ¹⁷N. Mironova-Ulmane, A. Kuzmin, I. Sildos, and M. Pärs, *Open Phys.* **9**, 1096 (2011).
- ¹⁸W. J. Duan, S. H. Lu, Z. L. Wu, and Y. S. Wang, *J. Phys. Chem. C* **116**, 26043 (2012).
- ¹⁹M. Marcuiš, M. Ristić, M. Ivanda, and S. Musić, *J. Alloys Compd.* **541**, 238 (2012).
- ²⁰A. C. Gandhi, J. Pant, S. D. Pandit, S. K. Dalimbkar, T.-S. Chan, C.-L. Cheng, Y.-R. Ma, and S. Y. Wu, *J. Phys. Chem. C* **117**, 18666 (2013).
- ²¹E. Aytan, B. Debnath, F. Kargar, Y. Barlas, M. M. Lacerda, J. X. Li, R. K. Lake, J. Shi, and A. A. Balandin, *Appl. Phys. Lett.* **111**, 252402 (2017), [arXiv:1710.06386](https://arxiv.org/abs/1710.06386).
- ²²M. M. Lacerda, F. Kargar, E. Aytan, R. Samnakay, B. Debnath, J. X. Li, A. Khitun, R. K. Lake, J. Shi, and A. A. Balandin, *Appl. Phys. Lett.* **110**, 202406 (2017).
- ²³M. Budde, C. Tschammer, P. Franz, J. Feldl, M. Ramsteiner, R. Goldhahn, M. Feneberg, N. Barsan, A. Oprea, and O. Bierwagen, *J. Appl. Phys.* **123**, 195301 (2018).
- ²⁴P. A. Fleury and R. Loudon, *Phys. Rev.* **166**, 514 (1968).
- ²⁵P. A. Fleury, *J. Appl. Phys.* **41**, 886 (1970).
- ²⁶D. J. Lockwood and G. J. Coombs, *J. Phys. C Solid State Phys.* **8**, 4062 (1975).
- ²⁷P. Schilbe, M. Ramsteiner, and K. H. Rieder, *J. Phys. Condens. Matter* **9**, 4979 (1997).
- ²⁸M. G. Cottam, *J. Phys. C Solid State Phys.* **5**, 1461 (1972).
- ²⁹W. Reichardt, V. Wagner, and W. Kress, *J. Phys. Condens. Matter* **8**, 3955 (1975).
- ³⁰M. G. Cottam and A. L. Awang, *J. Phys. C Solid State Phys.* **12**, 105 (1979).
- ³¹M. S. Kushwaha, *Physica* **112B**, 232 (1982).
- ³²A. Floris, S. de Gironcoli, E. K. U. Gross, and M. Cococcioni, *Phys. Rev. B* **84**, 161102 (2011).
- ³³M. Grimsditch, S. Kumar, and R. Goldman, *J. Magn. Magn. Mater.* **129**, 327 (1994).
- ³⁴H. Uchiyama, S. Tsutsui, and A. Q. R. Baron, *Phys. Rev. B* **81**, 241103 (2010).
- ³⁵T. I. Willett-Gies, C. M. Nelson, L. S. Abdallah, and S. Zollner, *J. Vac. Sci. Technol. A Vacuum, Surfaces, Film.* **33**, 061202 (2015).
- ³⁶R. Karsthof, M. Grundmann, A. M. Anton, and F. Kremer, *Phys. Rev. B* **99**, 235201 (2019).
- ³⁷M. Budde, T. Remmele, C. Tschammer, J. Feldl, P. Franz, J. Lähnemann, Z. Cheng, M. Hanke, M. Ramsteiner, M. Albrecht, and O. Bierwagen, *J. Appl. Phys.* **127**, 015306 (2020), <https://doi.org/10.1063/1.5129881>.